*Am J Physiol Cell Physiol*
281: C2049–C2060, 2001.

special communication

# LabHEART: an interactive computer model of rabbit ventricular myocyte ion channels and Ca transport

JOSÉ L. PUGLISI[1,2] AND DONALD M. BERS[2]
[1]*Department of Physiology and Biophysics, University of Illinois at Chicago, and* [2]*Department of Physiology, Loyola University Chicago, Stritch School of Medicine, Maywood, Illinois 60153*

Received 27 April 2001; accepted in final form 20 August 2001

**Puglisi, José L., and Donald M. Bers.** LabHEART: an interactive computer model of rabbit ventricular myocyte ion channels and Ca transport. *Am J Physiol Cell Physiol* 281: C2049–C2060, 2001.—An interactive computer program, LabHEART, was developed to simulate the action potential (AP), ionic currents, and Ca handling mechanisms in a rabbit ventricular myocyte. User-oriented, its design allows switching between voltage and current clamp and easy on-line manipulation of key parameters to change the original formulation. The model reproduces normal rabbit ventricular myocyte currents, Ca transients, and APs. We also changed parameters to simulate data from heart failure (HF) myocytes, including reduced transient outward ($I_{to}$) and inward rectifying K currents ($I_{K1}$), enhanced Na/Ca exchange expression, and reduced sarcoplasmic reticulum Ca-ATPase function, but unaltered Ca current density. These changes caused reduced Ca transient amplitude and increased AP duration (especially at lower frequency) as observed experimentally. The model shows that the increased Na/Ca exchange current ($I_{NaCa}$) in HF lowers the intracellular [Ca] threshold for a triggered AP from 800 to 540 nM. Similarly, the decrease in $I_{K1}$ reduces the threshold to 600 nM. Changes in $I_{to}$ have no effect. Combining enhanced Na/Ca exchange with reduced $I_{K1}$ (as in HF) lowers the threshold to trigger an AP to 380 nM. These changes reproduce experimental results in HF, where the contributions of different factors are not readily distinguishable. We conclude that the triggered APs that contribute to nonreentrant ventricular tachycardia in HF are due approximately equally (and nearly additively) to alterations in $I_{NaCa}$ and $I_{K1}$. A free copy of this software can be obtained at **http://www.meddean.luc.edu/lumen/DeptWebs/physio/bers.html**.

heart failure; excitation-contraction coupling; Na/Ca exchange; mathematical model

SINCE THE SEMINAL WORK of Hodgkin and Huxley (7) describing Na and K currents mathematically in squid axon, several groups have extended this sort of modeling to cardiac ionic currents and action potential (AP) (1, 14, 16–18). The tremendous increase of experimental work elucidating the behavior of ionic currents in heart (3) has required the development of new and more sophisticated models (4, 5, 11–13, 34).

Ca also plays a crucial role in cardiac excitation-contraction coupling (ECC) (2), and it has become clear that there is a dynamic interplay between the AP and Ca regulation mechanisms. The membrane potential ($E_m$) modulates Ca transport, and the Ca transient also can feedback to alter $E_m$. Thus cardiac cell models of AP and ionic currents have progressively incorporated more detailed formulations of the Ca transport systems.

A number of laboratories have made substantial contributions to this overall development (8, 18, 19, 23, 34, 35). However, the model of Luo and Rudy (12, 13, 35) has become, perhaps, the standard through the late 1990s. Unfortunate common features of most existing models are their limited flexibility and accessibility. As the model increases in complexity, it is more difficult to modify parameters, conditions, and equations. The accuracy required to reproduce a particular physiological observation can hinder the versatility of the whole model. Accessibility limitations pertain not only to obtaining the computer code but also to how user-friendly the interface is. A readily accessible model should be easy enough to use that *1*) students can quickly use it as a learning tool and *2*) researchers can use it as a development tool to test its fidelity in reproducing experimental results and also to explore potentially new experiments.

To fill this gap, we have created a computer program that combines current scientific findings with a user-friendly interface. We developed LabHEART, a program that is very intuitive to use and in which modifications of key variables, stimulation protocols, and default conditions can be made with a click on an icon.

Address for reprint requests and other correspondence: D. M. Bers, Dept. of Physiology, Loyola Univ. Chicago, Stritch School of Medicine, 2160 South First Ave., Maywood, IL 60153 (E-mail dbers@lumc.edu).

The costs of publication of this article were defrayed in part by the payment of page charges. The article must therefore be hereby marked "*advertisement*" in accordance with 18 U.S.C. Section 1734 solely to indicate this fact.

  

Table 1. *Ionic currents and Ca transport mechanisms*

| Mechanism | Symbol | Comments |
|---|---|---|
| Sarcoplasmic reticulum | | |
| Ca-ATPase, Ca release and buffering | SR | Same as Luo and Rudy |
| Na current | $I_{Na}$ | $G_{Na}$ set to 8 mS/μF |
| Na background current | $I_{Nab}$ | Same as Luo and Rudy |
| K currents | | |
| Transient outward | $I_{to}$ | Kinetics as in Ref. 34 with $G_{to}$ set to 0.060 mS/μF |
| Rapid repolarizing | $I_{K1}$ | $G_{K1}$ set to 0.540 ms/μF |
| Rapid delayed rectifier | $I_{Kr}$ | $G_{Kr}$ set to 0.035 mS/μF (see *Eqs. 4a–4e*) |
| Slow delayed rectifier | $I_{Ks}$ | $G_{Ks}$ decreased by 50% |
| Plateau current | $I_{Kp}$ | $G_{Kp}$ set to 0.008 mS/μF |
| Ca current (L-type) | $I_{Ca,L}$ | Same as Luo and Rudy |
| Ca current (T-type) | $I_{Ca,T}$ | Different kinetics from Luo and Rudy (see *Eqs. 3a–3e*) |
| Ca background current | $I_{Cab}$ | Same as Luo and Rudy |
| Cl current (Ca-activated) | $I_{Cl(Ca)}$ | Not included in Luo and Rudy (see *Eqs. 2a–2b*) |
| Na/Ca exchange | $I_{NaCa}$ | $K_{NaCa}$ set to 2,600 |
| Na-K-ATPase | $I_{NaK}$ | Same as Luo and Rudy |
| Sarcolemmal Ca pump | $I_{SLCa}$ | Same as Luo and Rudy |
| Ca Buffers | | Same as Luo and Rudy |

For details, refer to Luo and Rudy (12, 13, 35).

Standard electrophysiological plots, such as current-voltage relationships (*I-V* sets) or steady-state activation and inactivation curves are built-in features. Ionic concentrations and maximal current densities can be altered while the simulation is running, which adds a dynamic edge to the program.

A second key goal is that the model reproduces faithfully the electrophysiological and Ca transport characteristics of rabbit ventricular myocytes. Rabbit ventricle is used extensively in experimental studies, but there is no currently available model. A third goal is to simulate data obtained from control vs. heart failure (HF) rabbit ventricular myocytes where K currents, Na/Ca exchange, and sarcoplasmic reticulum (SR) Ca-ATPase function are altered (21, 22). While this study is, in part, a further test of the rabbit ventricular

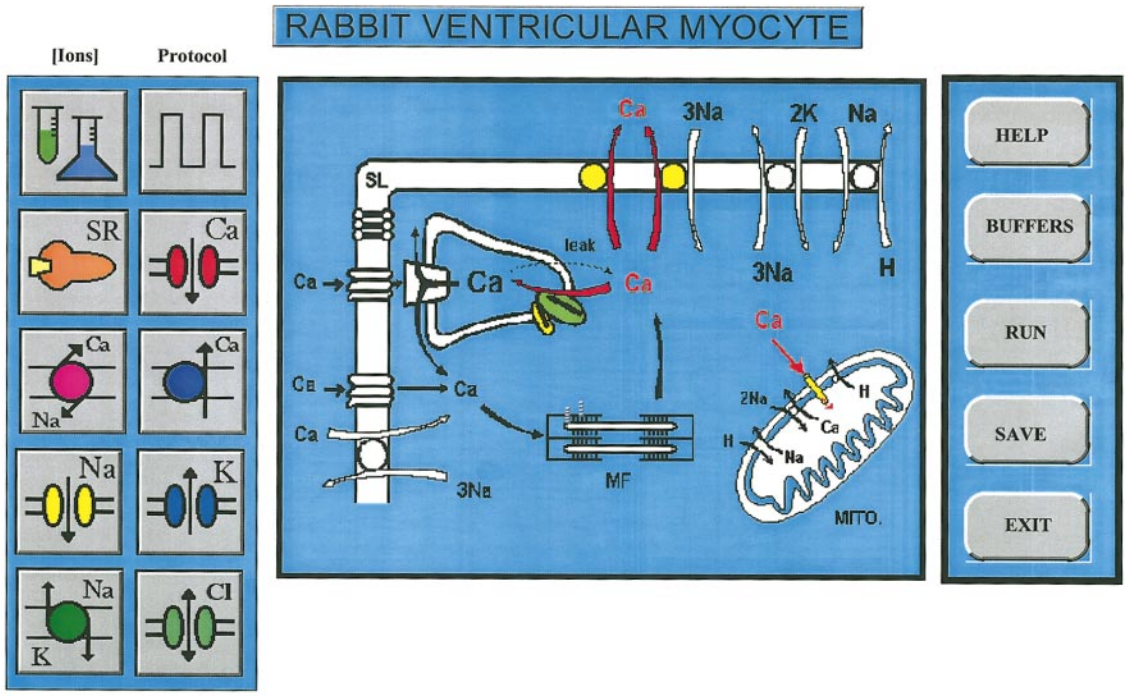


Fig. 1. The MAIN MENU screen shows a schematic diagram of the different mechanisms involved in cardiac excitation-contraction coupling (ECC) in a rabbit ventricular myocyte. SL, sarcolemma; Mito, mitochondrion; MF, myofilaments. By clicking on the icons located on the *left*, the user can *1*) establish ionic concentrations, *2*) set the stimulus waveforms, and visualize or alter *3*) characteristics of the sarcoplasmic reticulum (SR) or *4*) properties of Ca channels, *5*) Na/Ca exchange, *6*) sarcolemmal Ca pump, *7*) Na Channel, *8*) K channels, *9*) Na-K-ATPase, or *10*) Ca-activated Cl channel. By pressing the command buttons on the *right*, it is possible to obtain HELP screens, alter amounts of the Ca BUFFERS, RUN an action potential, SAVE a new set of default values under a new name, or EXIT the program.

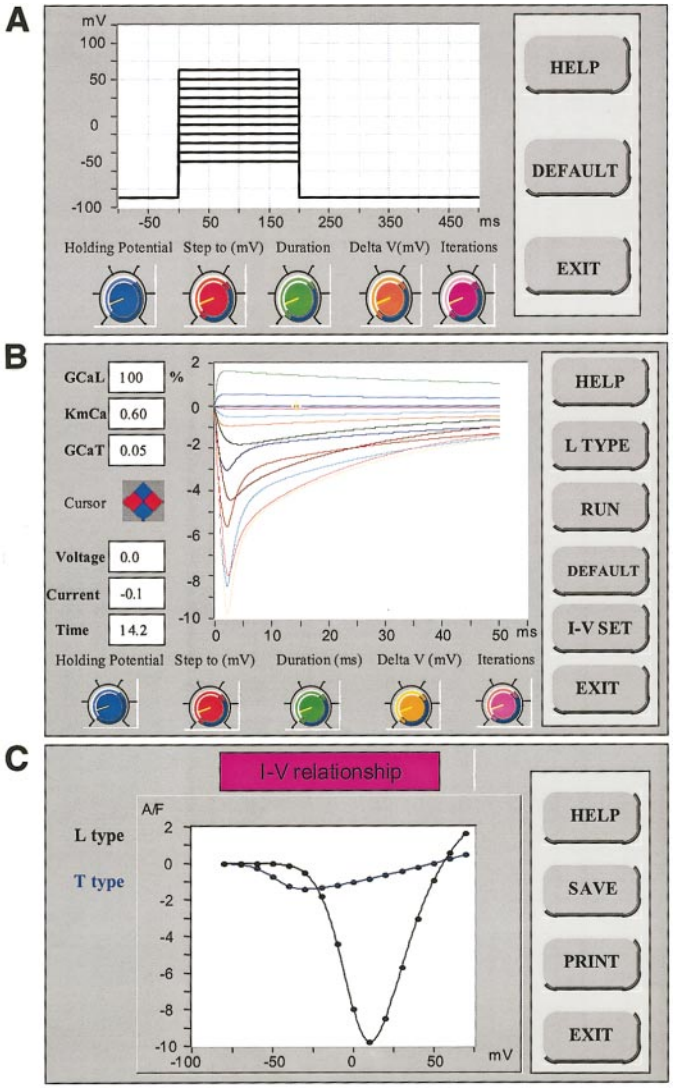


Fig. 2. Ca current in voltage clamp. *A*: schematic representation of the WAVEFORM screen used to control the protocol to generate current-voltage (*I-V*) data. The user inputs the values for holding potential, "step to" voltage, duration of pulse, voltage increments (Delta V), and the number of iterations. The screens shown here (and in Figs. 3 and 4) are simplified versions of the actual computer screen displays. For example, the "knobs" for adjusting parameters on the actual screen show numbers and units, and the selected value is also displayed in a box below the knob. The values also can be changed by either typing in values or nudging a cursor. *B*: $I_{Ca,L}$ traces obtained in the simulation. Conductances and affinity constant ($K_{mCa}$) values can be altered by typing the new values in the respective fields (*top left*). The cursor allows the user to choose a particular current trace and observe the corresponding values in boxes (*bottom left*). One can also switch protocol parameters by using the controls (*bottom*), without returning to the protocol screen. *C*: *I-V* screen showing superimposed $I_{Ca,L}$ and $I_{Ca,T}$ *I-V* relationships.

myocyte model, it also helps to better understand the cellular basis of changes in AP, Ca transients, and the observed propensity for triggered arrhythmias that lead to ventricular tachycardia in HF (23).

## MATERIALS AND METHODS

We adapted the equations from Luo and Rudy to rabbit ventricular myocytes using values obtained from the literature and from our laboratory. The model was implemented by using LabVIEW 5.0 graphical programming language from National Instruments (Austin, TX). Its inherent visual capabilities fit perfectly with our aim of intuitive use. We utilized the Rush and Larsen algorithm (26) to solve the set of differential equations. The main difference between our formulation and the one adopted by Luo and Rudy is the inclusion of transient outward K current ($I_{to}$) and Ca-activated Cl current [$I_{Cl(Ca)}$], as well as modification of the kinetics of T-type Ca channel ($I_{Ca,T}$), the rapid component of the delayed rectifier K current ($I_{Kr}$), and rescaling of several conductances to better match results in rabbit ventricle (see Table 1).

*Transient outward K current.* $I_{to}$ has been reported in rabbit ventricular myocytes (6, 9). It is also known as $I_{to1}$ to differentiate it from the Ca-activated Cl current [known as $I_{to2}$ or $I_{Cl(Ca)}$] that is activated at the same time during the AP (37). $I_{to}$ can contribute to ventricular repolarization. We used the $I_{to}$ formulation of Winslow et al. (34) for this current

$$I_{to} = G_{to} \times X_{to} \times Y_{to} \times (V - E_K) \quad (1a)$$

$$\alpha_{Xto} = 0.04561 \exp(0.03577 \times V) \quad (1b)$$

$$\beta_{Xto} = 0.0989 \exp(-0.06237 \times V) \quad (1c)$$

$$\alpha_{Yto} = 0.005415 \exp - [(V + 33.5)/5]/\{1 + 0.051335 \exp - [(V + 33.5)/5]\} \quad (1d)$$

$$\beta_{Yto} = 0.005415 \exp[(V + 33.5)/5]/\{1 + 0.051335 \exp[(V + 33.5)/5]\} \quad (1e)$$

where $G_{to}$ is the channel conductance, $X_{to}$ and $Y_{to}$ are activation and inactivation parameters, respectively, and $E_K$ is the reversal potential for K.

*Ca-activated Cl current.* $I_{Cl(Ca)}$ has been reported in rabbit Purkinje cells (30) and atrial (36) and ventricular myocytes (10). It is strongly temperature dependent, being very small at room temperature but substantial at 35°C (25). $I_{Cl(Ca)}$ can be suppressed by anion blockers such as DIDS or niflumic acid. Because of its Ca dependence, it also can be eliminated by blocking Ca current ($I_{Ca}$). We modeled this current as

$$I_{Cl(Ca)} = G_{Cl} \times (V - E_{Cl})/(1 + K_{mCa}/[Ca]_i) \quad (2)$$

where $G_{Cl}$ is the Cl conductance set to 10 mS/μF, $E_{Cl}$ is the reversal potential, and Ca dependence is incorporated as a Michaelis-Menten factor with $K_{mCa} = 0.10$ μM. These values were chosen to fit experimental records obtained by Puglisi et al. (25).

*T-type Ca current.* Although $I_{Ca,T}$ is not generally detectable in rabbit ventricular myocytes, we have included it to make a more complete theoretical model. The $I_{Ca,T}$ equations are

$$I_{Ca,T} = G_{Ca,T} \times b \times g \times (V - E_{Ca}) \quad (3a)$$

where $E_{Ca}$ is the Nernst potential for Ca and the gating parameters are as follows

$$b_\infty = 1/\{1 + \exp[-(V + 48)/6.1]\} \quad (3b)$$

$$\tau_b = 0.1 + (5.4/\{1 + \exp[(V + 100)/33]\}) \quad (3c)$$

$$g_\infty = 1/\{1 + \exp[(V + 66)/6.6)]\} \quad (3d)$$

$$\tau_g = 8 + (32/\{1 + \exp[(V + 65)/5)]\} \quad (3e)$$

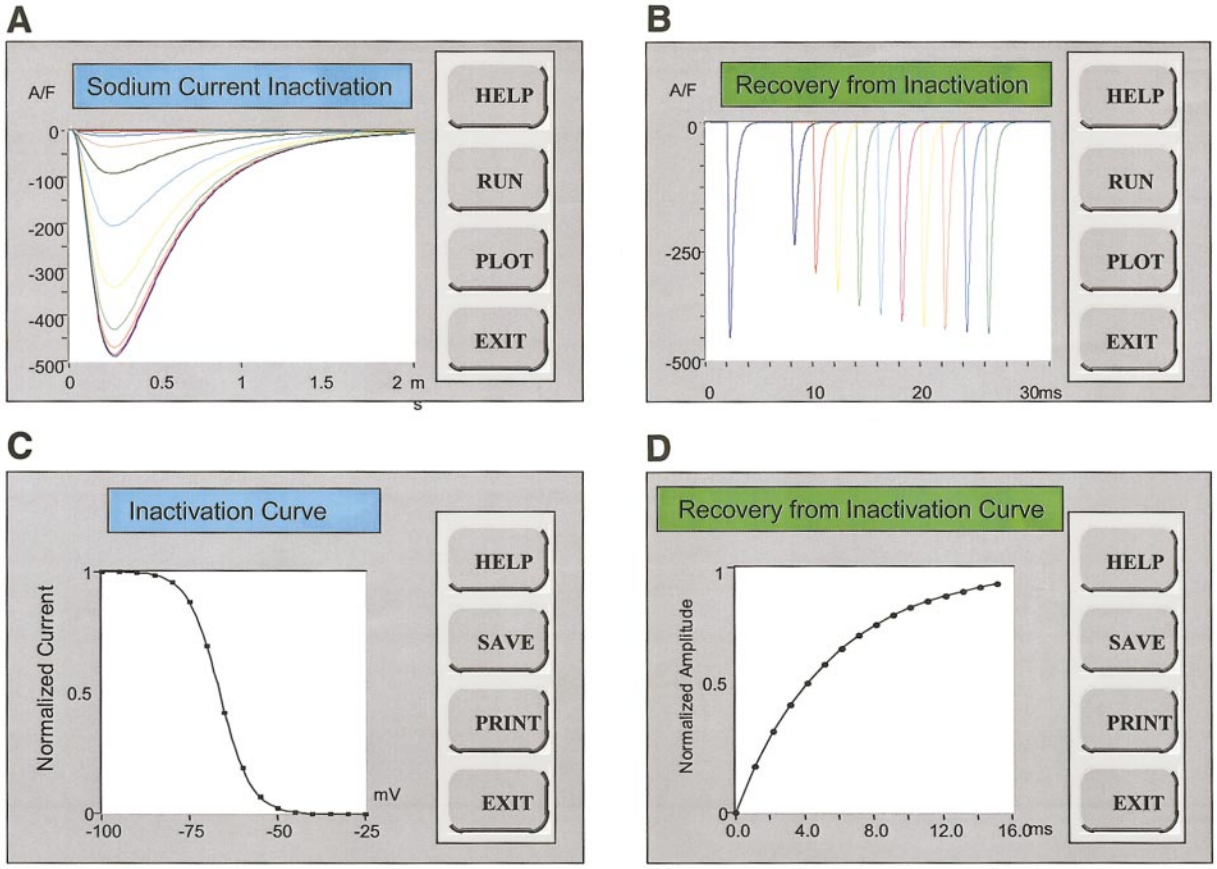


Fig. 3. Availability and recovery from inactivation. *A*: $I_{Na}$ availability traces for different holding membrane potentials ($E_m$). The PLOT command (*right*) generates the inactivation curve (*C*). *B*: recovery from $I_{Na}$ inactivation traces. Clicking the PLOT (*right*) command generates the recovery from inactivation curve (*D*). All graphs can be either saved or printed directly.

These equations are slightly different from those used by Zeng et al. (35), but they reproduce more accurately the *I-V* relationship for $I_{Ca,T}$.

The kinetics of $I_{Kr}$ were modified as follows

$$I_{Kr} = G_{Kr} \times X \times R \times (V - E_{Kr}) \quad (4a)$$

$$G_{Kr} = 0.02612 \times ([K]_o/5.4)^{0.5} \quad (4b)$$

$$X_\infty = 1/\{1 + \exp[-(V + 50)/7.5]\} \quad (4c)$$

$$R = 1/\{1 + \exp[(V + 33)/22.4]\} \quad (4d)$$

$$\tau_X = 1/(0.00138 \times (V + 7)/\{1 - \exp[-0.123 \times (V + 7)]\} + 0.00061 \times (V + 10)/(\exp\{0.145 \times [0.145 \times (V + 10)] - 1\} \quad (4e)$$

The rest of the parameters follow the same formulation as in Luo and Rudy, with some rescaling to better fit the rabbit myocyte characteristics (see Table 1).

The general scheme of LabHEART consists of a main menu (Fig. 1) from which the user can choose different tasks to perform. The main menu screen is a diagram with the major mechanisms involved in ECC, a series of icons (*left*), and a group of command buttons (*right*). The self-explanatory icons allow the user to alter the ionic concentration (*top left*), choose a voltage or current protocol (*top right*), or examine a particular mechanism, namely, SR, Ca channels, Na/Ca exchanger, sarcolemmal Ca-ATPase, Na and K channels, Na-K-ATPase, and $I_{Cl(Ca)}$. The command buttons allow the user to access help screens, alter the cytosolic buffers, run an AP or voltage-clamp simulation, save a particular set of conditions, or exit the program. During the generation of an AP, it is also possible to simulate SR Ca release induced by caffeine application and the effects of some drugs [e.g., nifedipine, almokalant, TTX, exchange inhibitory peptide, and 4-aminopyridine to simulate variable block of $I_{Ca}$, $I_{Kr}$, Na current ($I_{Na}$), Na/Ca exchange current ($I_{NaCa}$), and $I_{to}$]. One can choose either current-clamp protocols to simulate APs or voltage-clamp protocols to study individual current properties.

In every voltage-clamp simulation, typical plots such as *I-V* relationship or inactivation curves are built-in features. Also, bearing the novice user in mind, there are help options in each screen that explain possible choices and include a brief description of the mechanism under simulation or exploration. The default ionic concentrations were set as follows (in mM): $[Na]_o = 140$, $[Na]_i = 10$, $[K]_o = 5.4$, $[K]_i = 145$, $[Ca]_o = 1.8$, and resting $[Ca]_i = 120$ nM, where o indicates extracellular and i indicates intracellular concentration. Currents are expressed in amperes per farad and voltages in millivolts.

## RESULTS

*Voltage clamp and current characterization.* Under voltage-clamp mode, three protocols are available. The first protocol generates the *I-V* relationship of a chan-

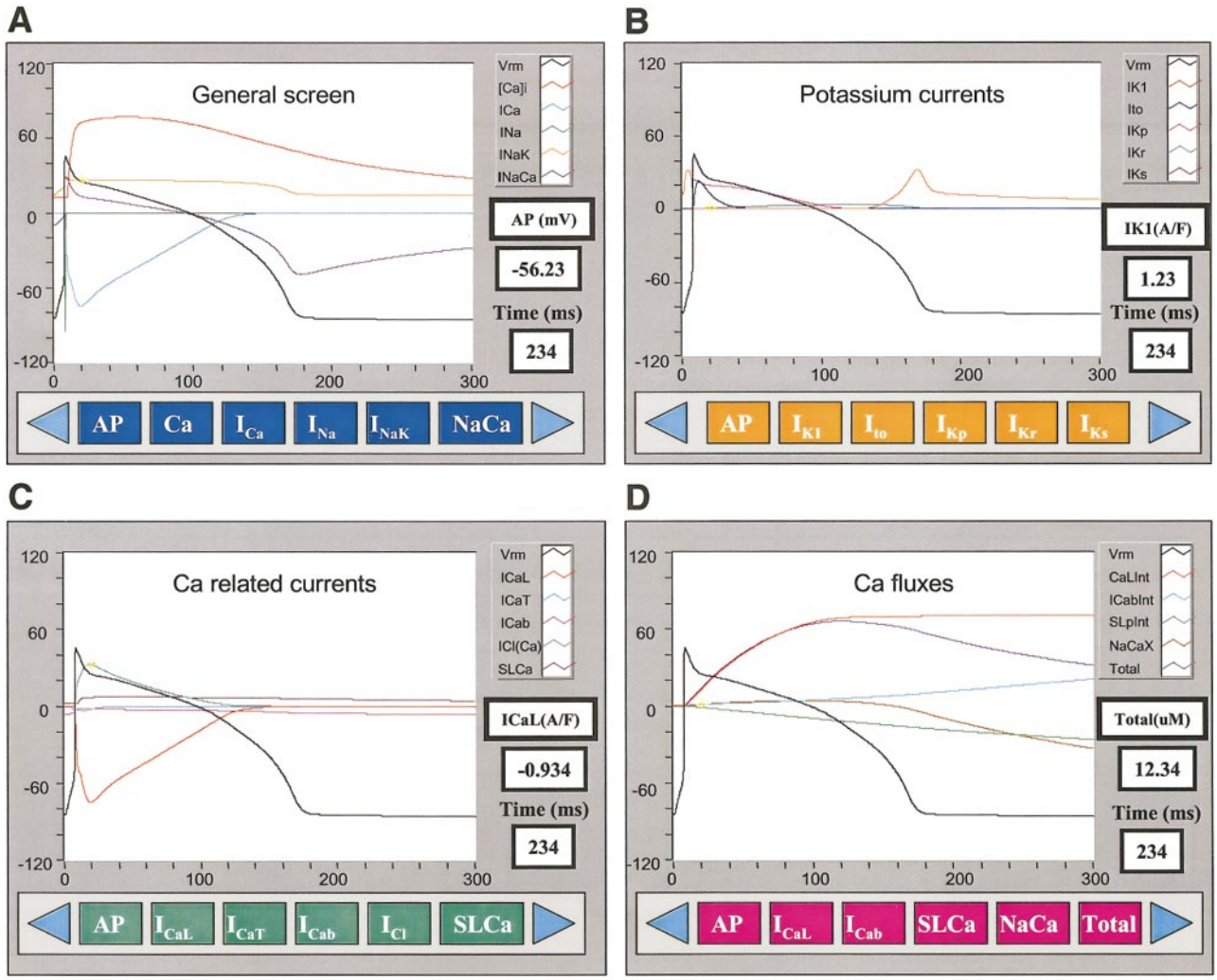


Fig. 4. Current clamp simulations: single pulse. *A*: simplified general screen of a default action potential (AP) simulation. This screen shows AP, intracellular Ca concentration ($[Ca]_i$), $I_{Ca}$, $I_{Na}$, $I_{NaK}$, and $I_{NaCa}$. Each of these traces can be toggled "on" or "off" by clicking the buttons below the display if the user wants to focus on a particular trace(s). *B*: K currents during the generation of an AP. *C*: Ca-related currents [$I_{Ca,L}$, $I_{Ca,T}$, $I_{Cab}$, $I_{Cl(Ca)}$, and the sarcolemmal Ca-pump current (SLCa)]. *D*: integrated amount of Ca transported by the Ca channels (L-type and background), Na/Ca exchange, and sarcolemmal Ca-ATPase. Transition between the different screens is achieved by pressing on the arrows located at the sides of the bar. Cursors also are on the screen (not shown here) that allow examination of values (with units) at any time point on any trace. The time scale also can be altered by overtyping with a new value (e.g., to expand the early part of the AP). All traces can be printed or saved as ASCII files.

nel. Figure 2 shows an example of this simulation for L- and T-type Ca channels. Figure 2*A* depicts the voltage waveforms used for this purpose. The protocol is set in a manner similar to experimental software; that is, the user selects the holding potential, "step to" voltage, duration of pulse, voltage increment (Delta V) between pulses, and number of iterations. Figure 2*B* illustrates the resulting L-type Ca current ($I_{Ca,L}$) traces. A particular current trace can be chosen with a cursor, and the specific current amplitude, voltage applied, and time of simulation appear on the screen (*left*). Some characteristics of the channel such as the conductance or the $K_m$ for Ca-induced inactivation can be altered by directly typing the new value in the corresponding field. The voltage protocol can be changed on this screen without returning to the previous one. Default conditions can be restored by a command button (*right*); the other command buttons allow the user to toggle between $I_{Ca,L}$ and $I_{Ca,T}$ or to quickly obtain the graph of the *I-V* set. Figure 2*C* shows superimposed *I-V* relationships for $I_{Ca,L}$ and $I_{Ca,T}$ and indicates the characteristic differences in amplitudes and voltage-dependence for those two channels. This plot can be either directly printed or saved as an ASCII file for further analysis or presentation. For the normal rabbit ventricular myocyte, the maximum T-type Ca channel conductance is set to zero, since no $I_{Ca,T}$ is seen in these cells. However, the option is there to include $I_{Ca,T}$, if it is observed under other conditions.

The second protocol under voltage clamp is the steady-state inactivation, or availability of the channel. Figure 3, *A* and *C*, shows this simulation for $I_{Na}$.

Once the $I_{Na}$ traces are obtained (Fig. 3*A*), the normalized peak amplitude of the current is plotted against the holding potential (Fig. 3*C*).

Another attribute of some ionic channels is the recovery from inactivation (assessed by the third voltage-clamp protocol, Fig. 3, *B* and *D*). The standard method to evaluate recovery is to use a first pulse to produce inactivation and a second pulse to assess the availability of the current, after rests of different durations and holding $E_m$. The time-dependent increase in test pulse $I_{Na}$ shows how the channel recovers from inactivation. The longer the interval between the pulses and the more negative the holding $E_m$, the faster the channel recovers. Figure 3*B* displays the $I_{Na}$ traces, and Fig. 3*D* shows the graph of recovery from inactivation. Like the *I-V* plot, this graph can be either directly printed or saved as an ASCII file for further analysis.

*Current clamp and AP simulations.* In current-clamp mode, there are three options: single pulse, double pulse, and run continuously. In the single pulse mode, an AP is generated by applying a single current pulse that can be adjusted by the user (e.g., to study threshold). The currents underlying the AP are shown in four consecutives screens (Fig. 4). The first screen is a general one (Fig. 4*A*) that exhibits AP, Ca transient, $I_{Ca,L}$, $I_{Na}$, Na-K-ATPase current ($I_{NaK}$), and $I_{NaCa}$. A second screen (Fig. 4*B*) shows all of the K currents included in the model ($I_{to}$, $I_{K1}$, $I_{Kr}$, $I_{Ks}$, and $I_{Kp}$). The third screen (Fig. 4*C*) portrays the Ca-related currents: $I_{Ca,L}$ and $I_{Ca,T}$, background Ca current ($I_{Cab}$), $I_{Cl(Ca)}$, and the sarcolemmal Ca-pump current. Finally, a fourth screen (Fig. 4*D*) illustrates the amount of Ca that has been transported across the membrane: the integral of Ca that entered through $I_{Ca,L}$, $I_{Cab}$, and $I_{NaCa}$, the amount of Ca extruded by the sarcolemmal Ca pump and $I_{NaCa}$, and also the net or total Ca flux. This value helps to show when Ca is being accumulated into the cell (total $>0$) or when the cell has been depleted of Ca (total $<0$). Figure 4*D* also shows that the total Ca that enters the cell is mainly due to $I_{Ca,L}$ and that the principal Ca extrusion mechanism is the Na/Ca exchange. In any of these four screens, each trace can be toggled on or off to focus on a particular aspect. Transition between these screens is accomplished by clicking the arrows on either side of the indicator bar. A particular trace can be chosen by a cursor, and its value is shown along with the appropriate units. The chosen traces, with their corresponding labels and scales, can be saved as an ASCII file. Figure 5 shows traces that have been exported and plotted using Prism 3.0 software (GraphPad). Figure 5*A* shows the AP and $[Ca]_i$. Figure 5*B* shows $I_{Na}$ with an inset to illustrate the temporal relationship between $E_m$, $I_{Na}$, and $I_{Ca,L}$ during the first 10 ms of the AP. Figure 5*C* displays superimposed traces of $I_{Ca,L}$, $I_{Ca,T}$, $I_{NaK}$, and $I_{NaCa}$, a combination that is not available in the four screens of this simulation. Finally, the five different K currents are presented in Fig. 5*D* with an inset of their behavior near the rapid upstroke of the AP. The single-pulse current-clamp mode also allows one to trigger SR Ca release directly at various times after the AP, thereby simulating spontaneous diastolic SR Ca release (or a caffeine-induced Ca transient). The second option (two pulses) follows the same design principles and is useful to study refractoriness. The third option (run continuously) presents the results as in a chart recorder, allowing the user to make on-line modifications of the ionic concentration to visualize the effects of some drugs.

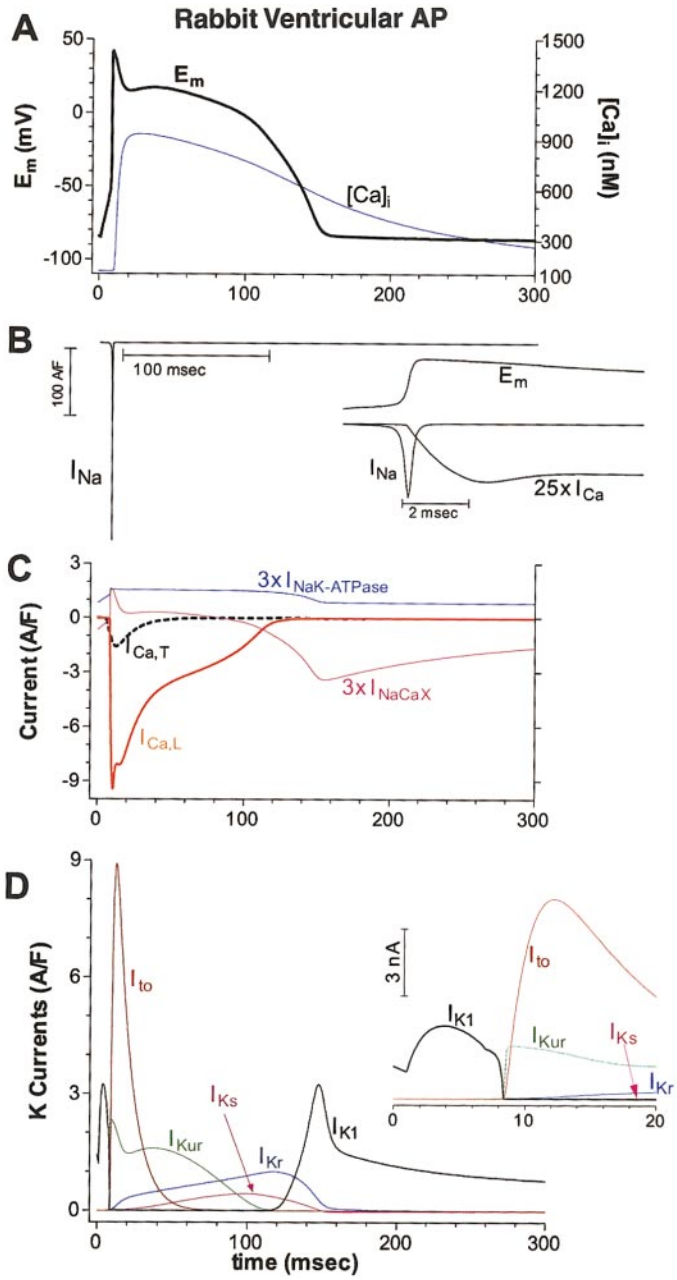


Fig. 5. Example of postprocessed AP traces. Different records were saved as ASCII files and plotted on selected scales. *A*: superimposed AP and $[Ca]_i$. *B*: $I_{Na}$ plotted alone and on an expanded time scale (*inset*) to show the temporal relationship of $E_m$, $I_{Na}$, and $I_{Ca,L}$ in the first 10 ms. *C*: AP, $I_{NaK}$ ($I_{NaK\text{-}ATPase}$), $I_{Ca,L}$, and $I_{NaCa}$ ($I_{NaCaX}$). This combination of traces is not present as a default condition but can be readily achieved this way. *D*: K currents, with an *inset* showing details at the onset of the AP.

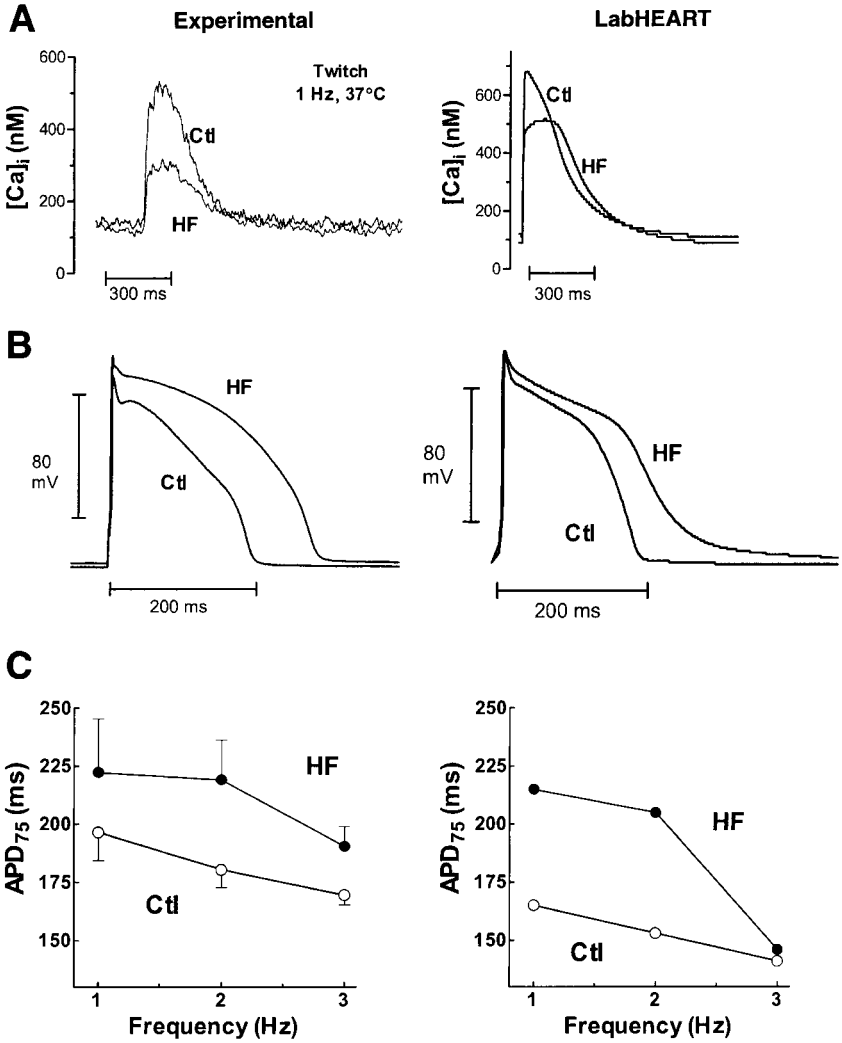


Fig. 6. Experimental data (*left*) and simulated traces (*right*) of control (Ctl) and heart failure (HF) myocytes. Default values for Na/Ca exchanger, $I_{K1}$, $I_{to}$, and SR Ca-pump rate were replaced with parameters measured in HF myocytes (see text). *A*: Ca transients. *B*: APs. *C*: effect of frequency on the AP duration ($APD_{75}$). Experimental data are from Ref. 22.

*Heart failure rabbit: a case study.* Current densities or maximal rate of Ca uptake ($V_{max}$) values can readily be adjusted, and we took advantage of this feature to simulate electrophysiological and Ca transport changes that we have measured in HF, which was induced by combined aortic insufficiency and aortic stenosis (21, 22). Ventricular myocytes from these HF rabbits exhibit 100% increase in $I_{NaCa}$, 24% reduction in SR Ca-ATPase function, 36% reduction in $I_{to}$, and 49% reduction in $I_{K1}$. Maximum conductance or $V_{max}$ values were changed, and this new HF parameter set can be saved and recalled at any time.

Figure 6, *A* and *B*, shows how the steady-state Ca transient and AP are modified in HF compared with control. The mean Ca transient amplitude was reduced by 40% experimentally (Fig. 6, *left*) and slightly less than this in the simulation (Fig. 6, *right*). The prolonged AP duration in HF (Fig. 6*C*) also was well reproduced by the model, as was the shortening with frequency and convergence of AP duration at higher frequency.

Figure 7*A* shows the $E_m$ dependence of $I_{NaCa}$ in HF and control myocytes. Both inward and outward current are increased twofold in HF (21). The apparent reversal potential is unchanged and close to the predicted value based on the pipette and extracellular solutions. Figure 7*B* illustrates Ca transients and $I_{NaCa}$ induced by a rapid caffeine application (31). In HF myocytes, a smaller Ca transient is accompanied by a higher $I_{NaCa}$. Figure 7*C* displays the Ca dependence of inward $I_{NaCa}$ on $[Ca]_i$. In HF, this current is much larger, indicating that $I_{NaCa}$ is functionally upregulated during dynamic Ca transient. The enhanced inward current means that Na/Ca exchange is extruding more Ca in direct competition with the SR Ca pump. This causes a lower SR Ca content that contributes to the smaller Ca transient. The experimental data in Fig. 7, *B* and *C*, were acquired at 23°C (rather than at 37°C as in the model data and all of Fig. 7*A*). This may largely account for the larger $I_{NaCa}$ values in the model and the more rapid decline of $[Ca]_i$ and inward $I_{NaCa}$ in the model (at 37°C) vs. the data at 23°C. Other factors that could impact on the precision of $I_{NaCa}$ predictions with the model are that *1*) LabHEART 4.7 uses a common cytosolic Ca pool, whereas submembrane $[Ca]_i$, in fact, may be higher than average $[Ca]_i$ during the SR Ca release (32), and *2*) the expression used for Na/Ca exchange in the model may

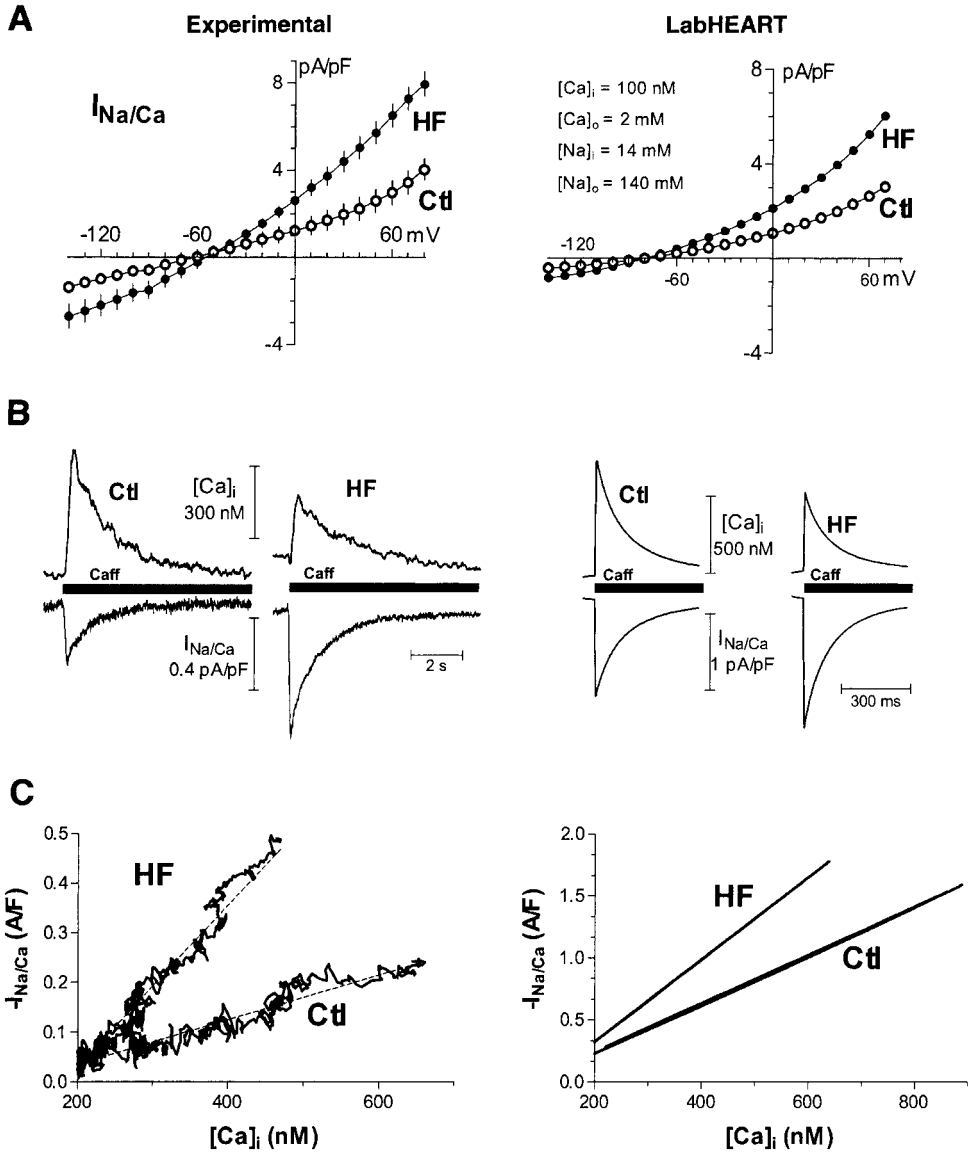


Fig. 7. Na/Ca exchange data (*left*) and simulations (*right*). *A*: $I_{NaCa}$ measured in control and HF myocytes (data from Ref. 21). *B*: caffeine (Caff)-induced Ca transient and $I_{NaCa}$ (data from Ref. 22). *C*: dynamic relation of $I_{NaCa}$ with Ca transient from *B* (data from Ref. 22). Experimental data were recorded at 37°C in *A* and at 23°C in *B* and *C*. Simulations with LabHEART were all at 37°C.

not have the correct dependence on $[Ca]_i$ (33). The higher $I_{NaCa}$ level in HF implies that for any given spontaneous SR Ca release [e.g., during a delayed afterdepolarization (DAD)], a greater inward $I_{NaCa}$ is expected. This could increase the likelihood that a DAD triggers an AP.

K currents also are altered in HF as shown in Fig. 8. $I_{to}$ is downregulated by 49% (Fig. 8, *A* and *B*). The faster inactivation kinetics in the simulation apparently result because the experimental data was recorded at 23°C, rather than at 37°C for the model. The inward rectifier current ($I_{K1}$) is also decreased (49%), as plotted in Fig. 8*C*. Again, the experimental data are at 23°C vs. the model at 37°C. Because experimental data have not always been recorded at 37°C, it would be convenient to be able to alter temperature in the model. Although we hope to include this option in future versions of LabHEART, this would be a major challenge, because there would be so many required parameters that might have different temperature dependence. Because $I_{K1}$ is important in stabilizing the resting $E_m$, the decreased $I_{K1}$ may facilitate depolarization during the initiation of triggered arrhythmias.

To further examine the role of altered $I_{NaCa}$ and $I_{K1}$ in triggered arrhythmias like DADs, we simulated DADs in a manner analogous to our experimental approach (Fig. 9). Pogwizd et al. (22) applied caffeine pulses at different SR Ca loads to determine the threshold amount of $[Ca]_i$ rise ($\Delta[Ca]_i$) required to produce a given depolarization ($\Delta E_m$) or trigger an AP. Using different frequencies to alter the SR Ca content, they determined that there was a greater depolarization for any give $\Delta[Ca]_i$ in HF, and the threshold $\Delta[Ca]_i$ to produce an AP was reduced by ~50% (515 ± 59 nM control, 280 ± 30 nM HF; Fig. 9*B*, *left*). In our model (Fig. 9*B*, right), caffeine application was simulated by opening the release channel and setting the $V_{max}$ for SR Ca uptake at zero. Moreover, because we can control the amount of SR Ca release directly, the model does not require the different conditioning pulses. De-

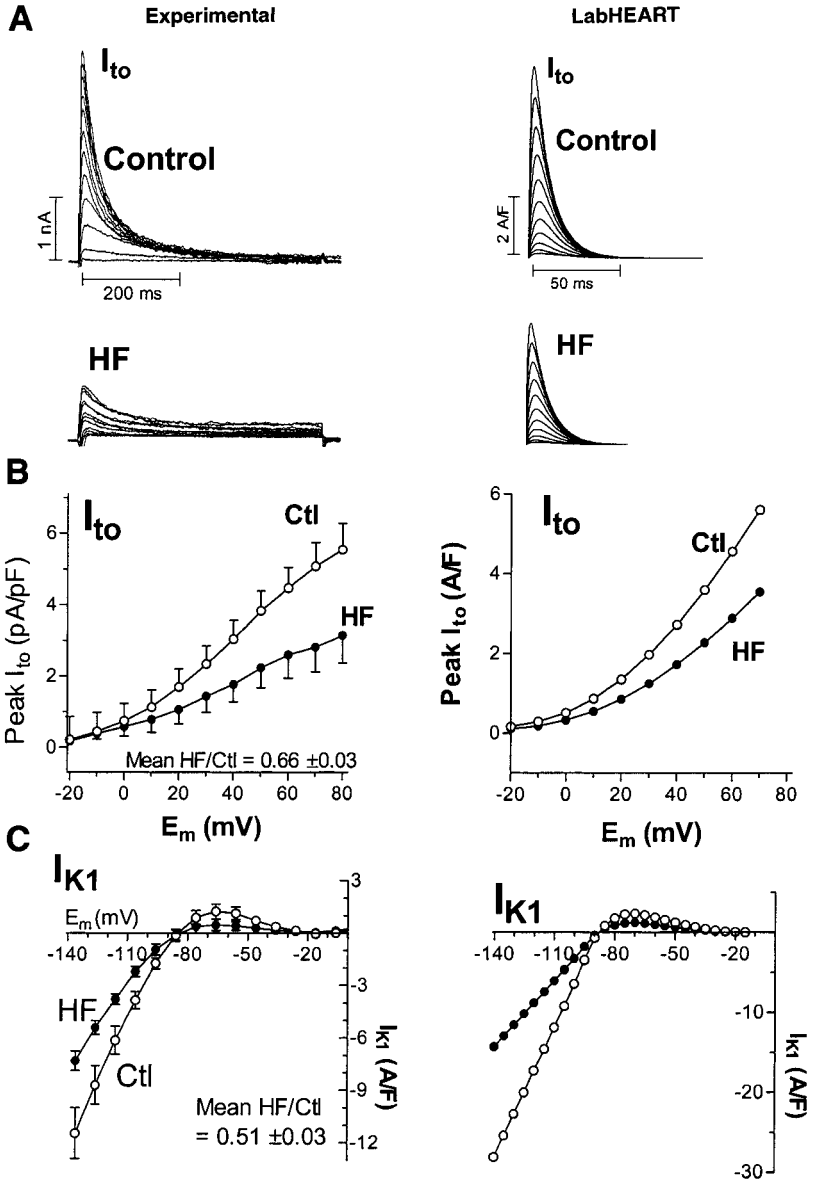


Fig. 8. K current alterations in HF. *A*: current traces of the $I_{to}$ for normal (*top*) and HF (*bottom*) myocytes. *B*: *I-V* relationship for $I_{to}$. *C*: *I-V* relationship for $I_{K1}$. Experiments were conducted at 23°C and simulations at 37°C. $I_{to}$ and $I_{K1}$ amplitudes used in the model were a compromise between these data (extrapolated to 37°C) and measurements from other studies and models at 37°C (notably, $I_{to}$ kinetics are faster and $I_{K1}$ amplitude is larger). NCX, Na/Ca exchange. Experimental data are from Ref. 22.

creasing $I_{K1}$ by 49% reduced the $\Delta[Ca]_i$ threshold by 25% [from 800 nM (control) to 600 nM]. When the Na/Ca exchange (NCX) was increased by 100%, the threshold value was reduced by 32% (540 nM). If these two changes are combined (as in HF), the $\Delta[Ca]_i$ threshold is reduced by 52% with respect to control (to 380 nM). These values are quite similar to the experimental observations in HF vs. control. The simulation also allows us to infer that the two key effects (increased NCX and reduced $I_{K1}$) contribute about equally and additively to the increased propensity for triggered arrhythmias in HF (24). The reduction of $I_{to}$ or SR Ca-ATPase seen in HF did not change DADs appreciably (not shown).

## DISCUSSION

The three goals achieved in this study were to *1*) create a new type of cardiac electrophysiology/Ca model that emphasizes the user interface, *2*) create a new model that predicts the electrophysiological and Ca transport properties of rabbit ventricular myocytes, and *3*) use this model to simulate and analyze altered function in an experimental model of HF in rabbits.

Computer models of this sort have two major aspects: elaboration and implementation. Elaboration of the equations that are used to describe the biological behavior of the channels and how they interact has been the focal point of most current cardiac AP models. Several excellent models have been developed for guinea pig, canine, and human ventricle and rabbit atrium (8, 11–13, 18, 23, 34, 35). Indeed, this is the context in which important mechanistic innovations in such models has almost invariably come. However, there is no currently available model for rabbit ventricular myocyte, a tissue that is widely used in many types of experimental studies. There are major differences in Ca transport, ionic currents, and APs among common species and cell types (2). In particular, rabbit

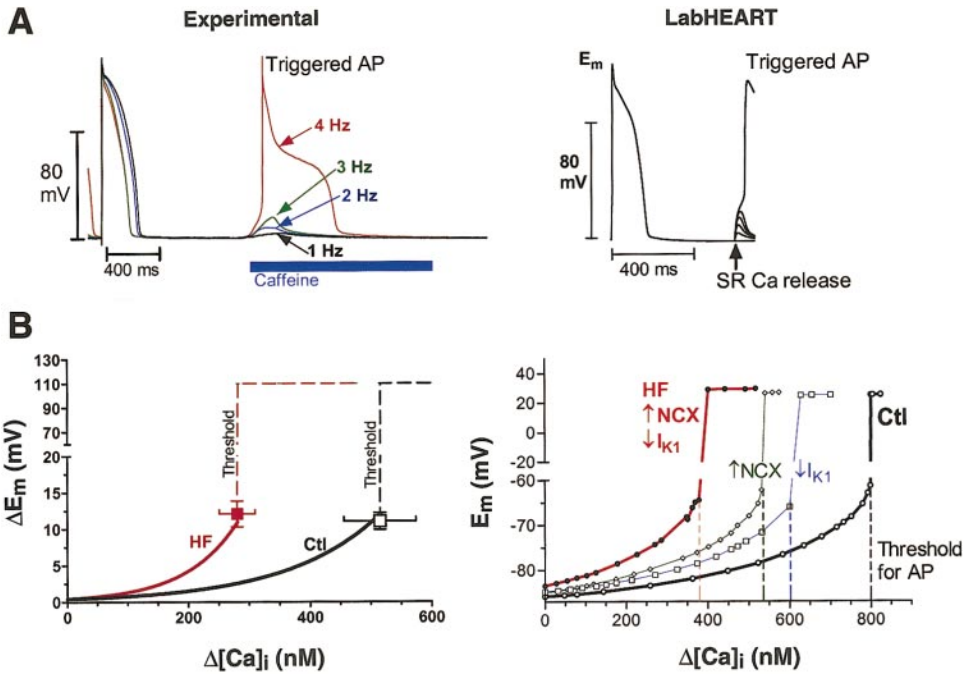


Fig. 9. In the current-clamp single-pulse mode, one can simulate spontaneous SR Ca release (as in a caffeine application). The amount of Ca released into the myoplasm is extruded by $I_{NaCa}$, producing a depolarizing current. *A*: for larger Ca releases, this current produces increasing depolarizations (eventually triggering an AP). *B*: we measured the delayed afterdepolarizations (DADs) for given amounts of Ca release for control and HF conditions. The amount of Ca needed to trigger a given DAD or an AP is significantly lower in the HF myocytes than in control (800 nM control, 380 nM HF). Experimental data are from Ref. 22.

ventricle has a different balance of K currents and AP shape (compared to rat, dog, human ventricle, and even rabbit atrium). The competition between the SR Ca-ATPase and Na/Ca exchange during $[Ca]_i$ decline also differs dramatically among these tissues. Thus it is important to have a computer model that is tailored to these specific properties.

The second aspect of computer models, implementation, refers to the computer program itself and, importantly, how the user interacts with the model. In the present study, we emphasize this aspect by modifying a widely utilized system of equations to simulate rabbit ventricular myocyte properties and also by creating a novel and highly user-friendly interface. LabHEART has several features that may allow it to have particularly broad utility. First, it is readily accessible. The program can be downloaded from our lab homepage (**http://www.meddean.luc.edu/lumen/DeptWebs/physio/bers.html**). Second, it runs well on a fairly basic personal computer. Some computer models for biological systems require more sophisticated computer resources that are not always readily available in the biology departments where many end users are located. Third, LabHEART is useful for students at many levels, including those with relatively limited background in electrophysiology or computer modeling. The help screens and intuitive layout of LabHEART encourage both exploration and learning. This will help students understand the principles and the dynamic interactions that occur among the systems considered. Fourth, LabHEART is valuable for the active scientist working in this field, where it may be particularly helpful in developing new experimental hypotheses or insights. Indeed, the user may freely adjust ionic conditions, pulse protocols, and some ion channel properties. Thus the experimentalist does not have to independently develop an integrative model to study the impact of more discretely measured electrophysiological changes. Fifth, LabHEART is relatively up to date with respect to ion currents and Ca transport properties.

Using this new program, we were able to both simulate and analyze the mechanisms underlying the generation of triggered arrhythmias in HF myocytes. Electrical reentry can contribute to ventricular tachycardia in many pathophysiological states, but three-dimensional mapping studies show that most fatal arrhythmias in HF initiate by nonreentrant mechanisms such as DADs (20). By altering the default values of the $I_{K1}$, $I_{to}$, $I_{NaCa}$, and the SR Ca-ATPase in the manner measured in voltage clamp and Ca transient studies (21,22), we could simulate the changes in AP and Ca transients. Furthermore, by adjusting these parameters individually in LabHEART (in a manner that cannot be done readily in experiments), we could analyze the likely quantitative contributions of different changes to the size of DADs for a given spontaneous SR Ca release (and the $\Delta[Ca]_i$ threshold for triggering an AP). We found that the reduced $I_{K1}$ and enhanced $I_{NaCa}$ contribute about equally to shifts in $[Ca]_i$ dependence of DADs and AP threshold (25–32% shifts of threshold $\Delta[Ca]_i$). Moreover, these two effects seem to be approximately additive, because when both changes are instituted together, the threshold $\Delta[Ca]_i$ is reduced by 52% (and this matches the experimental observations where the two contributions cannot be readily differentiated) (22). This is only one example of the kind of additional analytical insight that can be gleaned from a computer model of this type.

It should also be acknowledged that this is an ongoing process and that LabHEART 4.7 as described here is a first major step on this path. We are actively

developing new scientific expressions for modeling the ventricular AP and Ca transients (e.g., more appropriate equations for SR Ca transport and Na/Ca exchange) (28, 29, 33). Several ionic currents also need additional refinement. For example, there are at least two molecular contributors to $I_{to}$ (15) that have different kinetics. Altered functional frameworks also will be necessary. For instance, it is clear that local $[Ca]_i$ near the sarcolemma differs from the bulk $[Ca]_i$ and possibly also from $[Ca]_i$ in the cleft between junctional SR and the sarcolemma (32). We have begun preliminary incorporation of some of these novel aspects into the elaboration phase (27) and plan to eventually transport that much more complex model into the user-friendly LabHEART format. A long-term challenge is to allow the LabHEART user to readily simulate different cell types (from stored parameter sets) and also to be able to easily change the basic equations used for different channels, transporters, or buffers.

We are grateful to Dr. T. R. Shannon for valuable comments on the manuscript.

This work was supported in part by American Heart Association Fellowship 9920452Z (to J. L. Puglisi), National Heart, Lung, and Blood Institute Grant HL-30077 (to D. M. Bers), and the National Space Biomedical Research Institute (to D. M. Bers).

## REFERENCES

1. **Beeler GW and Reuter H.** Reconstruction of the action potential of ventricular myocardial fibers. *J Physiol* 268: 177–210, 1977.
2. **Bers DM.** *Excitation-Contraction Coupling and Cardiac Contractile Force* (2nd ed.). Dordrecht, The Netherlands: Kluwer Academic, 2001, p. 427.
3. **Carmeliet E.** Cardiac ionic currents and acute ischemia: From channels to arrhythmias. *Physiol Rev* 79: 917–1017, 1999.
4. **Di Francesco D and Noble D.** A model of cardiac electrical activity incorporating ionic pumps and concentration changes. *Phil Trans R Soc Lond* 307: 353–398, 1985.
5. **Hilgemann DW and Noble D.** Excitation-contraction coupling and extracellular calcium transients in rabbit atrium: reconstruction of basic cellular mechanisms. *Phil Trans R Soc Lond* 230: 163–205, 1987.
6. **Hiraoka M and Kawano S.** Calcium-sensitive and insensitive transient outward current in rabbit ventricular myocytes. *J Physiol* 410: 187–212, 1989.
7. **Hodgkin L and Huxley AF.** A quantitative description of membrane currents and its application to conduction and excitation in nerve. *J Physiol* 117: 500–544, 1952.
8. **Jafri MS, Rice JJ, and Winslow RL.** Cardiac Ca dynamics: the roles of ryanodine receptor adaptation and sarcoplasmic reticulum load. *Biophys J* 74: 1149–1168, 1998.
9. **Kawano S and Hiraoka M.** Transient outward currents and action potentials alterations in rabbit ventricular myocytes. *J Mol Cell Cardiol* 23: 681–693, 1991.
10. **Kawano S, Hirayama Y, and Hiraoka M.** Activation mechanism of Ca sensitive outward current in rabbit ventricular myocytes. *J Physiol* 486: 593–604, 1995.
11. **Lindblad DS, Murphy CR, Clark JW, and Giles WR.** A model of the action potential and underlying membrane currents in a rabbit atrial cell. *Am J Physiol Heart Circ Physiol* 271: H1666–H1696, 1996.
12. **Luo CH and Rudy Y.** A model of the ventricular cardiac action potential, depolarization, repolarization and their interaction. *Circ Res* 68: 1501–1526, 1991.
13. **Luo CH and Rudy Y.** A dynamic model of the cardiac ventricular action potential. I. Simulations of ionic currents and concentration changes. *Circ Res* 74: 1071–1096, 1994.
14. **McAllister RE, Noble D, and Tsien RW.** Reconstruction of the electrical activity of cardiac Purkinje fibres. *J Physiol* 251: 1–59, 1975.
15. **Nerbonne JM.** Molecular basis of functional voltage-gated $K^+$ channel diversity in the mammalian myocardium. *J Physiol* 525: 285–298, 2000.
16. **Noble D.** A modification of the Hodgkin-Huxley equations applicable to Purkinje fibre action and pacemaker potential. *J Physiol* 160: 317–352, 1962.
17. **Noble D and Tsien RW.** The kinetics and rectifier properties of the slow potassium current in cardiac Purkinje fibers. *J Physiol* 195: 185–214, 1968.
18. **Nordin C.** Computer model of membrane current and intracellular Ca flux in the isolated guinea pig ventricular myocytes. *Am J Physiol Heart Circ Physiol* 265: H2117–H2136, 1993.
19. **Nygren A, Fiset C, Firek L, Clark JW, Lindblad DS, Clark RB, and Giles WR.** Mathematical model of an adult human atrial cell. The role of K currents in repolarization. *Circ Res* 82: 63–81, 1998.
20. **Pogwizd SM, Chung MK, and Cain ME.** Termination of ventricular tachycardia in the human heart: insights from three-dimensional mapping of nonsustained ventricular tachycardias. *Circulation* 95: 2517–2527, 1997.
21. **Pogwizd SM, Qi M, Yuan W, Samarel AM, and Bers DM.** Upregulation of Na/Ca exchanger expression and function in an arrhythmogenic rabbit model of heart failure. *Circ Res* 85: 1009–1019, 1999.
22. **Pogwizd SM, Schlotthauer K, Li L, Yuan W, and Bers DM.** Arrhythmogenesis and contractile dysfunction in heart failure: roles of sodium-calcium exchange, inward rectifier potassium current and β-adrenergic responsiveness. *Circ Res* 88: 1159–1167, 2001.
23. **Priebe L and Beuckelman DJ.** Simulation study of cellular electric properties in heart failure. *Circ Res* 82: 1206–1223, 1998.
24. **Puglisi JL, Pogwizd SM, Yuan W, and Bers DM.** Increased Na/Ca exchange and reduced $I_{K1}$ facilitate triggered action potentials in a rabbit model of heart failure (Abstract). *Biophys J* 78: 55A, 2000.
25. **Puglisi JL, Yuan W, Bassani JWM, and Bers DM.** Ca influx through Ca channels in rabbit ventricular myocytes during action potential clamp. *Circ Res* 85: e7-e16, 1999.
26. **Rush S and Larsen H.** A practical algorithm for solving dynamic membrane equations. *IEEE Trans Biomed Eng* 25: 389–392, 1978.
27. **Shannon TR and Bers DM.** A mathematical model describes the SR load-dependence of Ca dynamics in cardiac myocytes (Abstract). *Biophys J* 80: 594A, 2001.
28. **Shannon TR, Ginsburg KS, and Bers DM.** Reverse mode of the sarcoplasmic reticulum calcium pump and load-dependent cytosolic calcium decline in voltage-clamped cardiac ventricular myocytes. *Biophys J* 78: 322–333, 2000.
29. **Shannon TR, Ginsburg KS, and Bers DM.** Potentiation of fractional sarcoplasmic reticulum calcium release by total and free intra-sarcoplasmic reticulum calcium concentration. *Biophys J* 78: 334–343, 2000.
30. **Sipido KR, Callewaert G, and Carmeliet E.** $[Ca]_i$ transients and $[Ca]_i$-dependent chloride current in single Purkinje cells from rabbit heart. *J Physiol* 468: 641–667, 1993.
31. **Trafford AW, Diaz ME, and Eisner DA.** A novel, rapid and reversible method to measure Ca buffering and time course of total sarcoplasmic reticulum Ca content in cardiac ventricular myocytes. *Pflügers Arch* 437: 501–503, 1999.
32. **Trafford AW, Diaz ME, O'Neill SC, and Eisner DA.** Comparison of subsarcolemmal and bulk calcium concentration during spontaneous calcium release in rat ventricular myocytes. *J Physiol* 488: 577–586, 1995.
33. **Weber CR, Ginsburg KS, Philipson KD, Shannon TR, and Bers DM.** Allosteric regulation of Na/Ca exchange current by cytosolic Ca in intact cardiac myocytes. *J Gen Physiol* 117: 119–131, 2001.
34. **Winslow RL, Rice J, Jafri S, Marban E, and O'Rourke B.** Mechanisms of altered excitation-contraction coupling in canine

tachycardia-induced heart failure. II. Model studies. *Circ Res* 84: 571–586, 1999.
35. **Zeng J, Laurita R, Rosenbaum DS, and Rudy Y.** Two components of the delayed rectifier K currents in ventricular myocytes of the guinea pig type: theoretical formulation and their role in repolarization. *Circ Res* 77: 140–152, 1995.
36. **Zygmunt AC and Gibbons WR.** Calcium-activated chloride current in rabbit ventricular myocytes. *Circ Res* 68: 424–437, 1991.
37. **Zygmunt AC and Gibbons WR.** Properties of the calcium-activated chloride current in heart. *J Gen Physiol* 99: 391–414, 1992.